Renormalization of the weak hadronic current in the nuclear medium

T. Siiskonen*
Helsinki Institute of Physics, University of Helsinki, P.O. Box 9, FIN-00014 Helsinki, Finland

M. Hjorth-Jensen
Department of Physics, University of Oslo, N-0316 Oslo, Norway

J. Suhonen
Department of Physics, University of Jyväskylä, P.O. Box 35, FIN-40351 Jyväskylä, Finland
(Received 15 December 2000; published 12 April 2001)

The renormalization of the weak charge-changing hadronic current as a function of the reaction energy release is studied at the nucleonic level. We have calculated the average quenching factors for each type of current (vector, axial vector, and induced pseudoscalar). The obtained quenching in the axial vector part is, at zero momentum transfer, 19% for the $1s0d$ shell and 23% in the $1p0f$ shell. We have extended the calculations also to heavier systems such as ^{56}Ni and ^{100}Sn, where we obtain stronger quenchings, 44% and 59%, respectively. Gamow-Teller-type transitions are discussed, along with the higher-order matrix elements. The quenching factors are constant up to roughly 60 MeV momentum transfer. Therefore the use of energy-independent quenching factors in beta decay is justified. We also found that going beyond the zeroth and first order operators (in inverse nucleon mass) does not give any substantial contribution. The extracted renormalization to the ratio C_P/C_A at $q=100$ MeV is -3.5%, -7.1%, -28.6%, and $+8.7\%$ for mass 16, 40, 56, and 100, respectively.

DOI: 10.1103/PhysRevC.63.055501 PACS number(s): 21.30.Fe, 23.40.−s, 21.60.Cs, 21.10.Pc

I. INTRODUCTION

The phenomenological structure of the weak hadronic current between proton and neutron states is well determined by its properties under the Lorentz transformation. The additional constraints come from the requirement of time reversal symmetry as well as from the invariance under the G-parity transformation (combined charge conjugation and isospin rotation). The resulting interaction Hamiltonian consists of vector (V), axial vector (A), induced weak magnetism (M), and induced pseudoscalar (P) terms together with the associated form factors C_α, $\alpha=V$, A, M, or P. These form factors are called as coupling constants at zero momentum transfer. The present experimental knowledge does not exclude the presence of the scalar and tensor interactions. However, their contribution is expected to be small due to weak couplings [1].

The values of vector, axial vector, and weak magnetism couplings are well established by beta-decay experiments as well as by the conserved vector current (CVC) hypothesis, introduced already in the late 1950s [2]. The magnitude of the pseudoscalar coupling is more uncertain, although the partially conserved axial current (PCAC) hypothesis [3] provides an estimate along with muon capture experiments in hydrogen [4,5]. The value of C_P in the nuclear medium is not precisely established.

In nuclear beta decay, with an energy release up to some 20 MeV, only the vector (Fermi) and the axial vector (Gamow-Teller) terms are usually important. The induced pseudoscalar and weak magnetism parts are essentially inactive, since their contributions are proportional to q/M, where q is the energy release and M is the nucleon mass (in units where $\hbar=c=1$). There are, however, weak nuclear processes, like muon capture, where the energy release is much higher (in muon capture, typically $q\approx m_\mu\approx 100$ MeV).

Summed theoretical beta-decay strengths are systematically larger than the experimental ones. This so-called quenching of the (allowed) decay strength is usually explained in terms of core polarization (degrees of freedom which are left out from the model space) and non-nucleonic degrees of freedom like isobars and meson-exchange currents [6]. The core polarization correction is intimately linked to the choice of the model space (the orbits between the inert core and excluded orbits at high single-particle energies). Hence, to demonstrate this dependence, we have used two different model spaces for the nuclei in the middle of the $1p0f$ shell, like Cu and Zn isotopes (see below).

In [7,8] we have self-consistently constructed effective operators for the weak hadronic current between proton and neutron states. These operators, as explained in Sec. III, take into account the above-mentioned core polarization effects, which are expected to be the largest correction to the bare matrix elements [9]. Earlier, many authors (e.g., [6,10–12]) established the quenching factors for the Gamow-Teller decays and closely related magnetic dipole ($M1$) transitions. In the present work our aim is to calculate self-consistently the quenching for all types of operators (V, A, M, and P) for energies up to the muon capture range. In addition to $1s0d$ and $1p0f$ shells, we have extended our calculations to $^{56}_{28}$Ni and $^{100}_{50}$Sn as closed-shell cores.

Empirically, one expects about 20% quenching of the axial vector part in the $1s0d$ shell; i.e., the calculated Gamow-Teller matrix elements $\langle\sigma\rangle$ are to be multiplied by a factor of ~ 0.8 [11] when both core polarization and non-

*Mailing address: EP Division, CERN, CH-1211 Geneva 23, Switzerland.

nucleonic degrees are accounted for.[1] Effects of the same magnitude are expected in the $1p0f$ shell [12], and the mass dependence of the quenching is seemingly saturated. However, the major shell closures which separate the spin-orbit partners in our ^{56}Ni and ^{100}Sn model spaces introduce large first-order corrections to the operators. Thus, the situation is not analogous to the one seen in light nuclei with closed LS shells. For a recent work in the Sn mass region, see, e.g., Ref. [13].

We remind the reader that the quenching we describe is always related to the choice of the model space. This means that if a shell-model calculation is to be performed for, say, Cu or Zn isotopes with ^{56}Ni as closed-shell core, a pertinent model space consists then of the single-particle orbits $0f_{5/2}$, $1p_{1/2}$, $1p_{3/2}$, and $0g_{9/2}$. If transition probabilities are to be calculated, then effective operators defined for this model space are to be used. Disagreement with experiment may often imply missing degrees of freedom. Typically, for nuclei with mass numbers close to $A=56$, particle-hole excitations involving the $0f_{7/2}$ hole orbit may be important. Then, the model space needs to be enlarged and the corresponding effective operator to be computed.

Our extracted quenching factors are averaged over the model space single-particle orbits (see Sec. IV). Thus, they are not directly applicable for the closed-shell plus one nucleon configurations, like ^{17}O. Instead, they should be used in configuration-mixing calculations (shell model in particular) in the indicated model space. Strictly speaking, in this case, also effective two-body operators should be calculated. In practice, this is rarely done and accordingly we neglect such corrections. For reference, we shall also give the renormalizations of some single-particle transitions.

The nuclear muon capture can be used for the extraction of the ratio C_P/C_A. Unfortunately, the results for partial capture rates are very sensitive to the applied nuclear model, especially to the residual two-body interaction (see, e.g., [14] and references therein). The total rates offer perhaps a more reliable source of information, indicating no or only small quenching for the ratio C_P/C_A [15]. It is of interest to see whether this can be explained in terms of effective charges for the axial vector and pseudoscalar operators, that is, without the complications coming from the nuclear structure calculations.

In addition to the zeroth-order Fermi and Gamow-Teller-type operators, our set includes the first-order terms in the transition amplitude (first order in q/M as well as velocity-dependent terms). We shall also examine the importance of the second-order terms. We stress that the results obtained in this work can be applied quite generally. We have used the muon as an initial bound-state lepton, but the results apply to electron capture as well and therefore to beta decay in general (in our calculations, the muon is nothing but a heavy electron).

In this work, after a short review of the formalism of the semileptonic weak processes in Sec. II and effective operators in Sec. III, we concentrate on the results in Sec. IV. We consider four cases, with ^{16}O, ^{40}Ca, ^{56}Ni, and ^{100}Sn as closed-shell cores.

II. INVARIANT AMPLITUDE AND SINGLE-PARTICLE OPERATORS

After the standard nonrelativistic reduction, the semileptonic charge-changing weak process

$$\lambda_b + p \rightarrow \nu_\lambda + n, \tag{1}$$

where λ_b is a bound (anti)lepton in an atomic $1S$ orbit and ν_λ is the corresponding (anti)neutrino, is described by the amplitude

$$\mathcal{M}^2 = \sum_{\kappa u} |M_V(\kappa,u) + M_A(\kappa,u) + M_P(\kappa,u)|^2. \tag{2}$$

We take λ_b to be a muon, with a mass $m_\mu = 105.658$ MeV. The form of the effective weak hadronic current used for Eq. (2) is the most general one consistent with the expected G-parity symmetry and time reversal symmetry. The functions $M_\alpha(\kappa,u)$ include the form factors, transition operators, and angular momentum couplings. Explicitly, the vector part is given by

$$\begin{aligned} M_V(\kappa,u)/C_V(q^2) = {} & [0lu] S_{0u}(\kappa)\delta_{lu} - \frac{1}{M}[1\bar{l}up] S'_{1u}(-\kappa) + \frac{q\sqrt{3}}{2M} \\ & \times \left\{ \sqrt{\frac{\bar{l}+1}{2\bar{l}+3}}[0\bar{l}+1u+]\delta_{\bar{l}+1,u} + \sqrt{\frac{\bar{l}}{2\bar{l}-1}}[0\bar{l}-1u-]\delta_{\bar{l}-1,u} \right\} S'_{1u}(-\kappa) \\ & + \sqrt{\frac{3}{2}}\frac{q}{M}(1+\mu_p-\mu_n)\{\sqrt{\bar{l}+1}\, W(11u\bar{l},1\bar{l}+1)[1\bar{l}+1u+] \\ & + \sqrt{\bar{l}}\, W(11u\bar{l},1\bar{l}-1)[1\bar{l}-1u-]\} S'_{1u}(-\kappa). \end{aligned} \tag{3}$$

[1] The Gamow-Teller strengths $B(\mathrm{GT}) \propto \langle\sigma\rangle^2$ are then multiplied by $(0.8)^2$.

We consider the V and M terms together, as suggested by the CVC hypothesis: $C_M=(\mu_p-\mu_n)C_V/2M$, where μ_p and μ_n are the anomalous magnetic moments of the proton and neutron in nuclear magnetons. The Fermi-type term is the first term on the right-hand side of Eq. (3). The axial vector part is given by

$$M_A(\kappa,u)/C_A(q^2)=-[1lu]S_{1u}(\kappa)+\frac{1}{M}[0\bar{l}up]\delta_{\bar{l}u}S'_{0u}(-\kappa) - M_P(\kappa,u)/C_P(q^2), \tag{4}$$

including the pseudoscalar part

$$M_P(\kappa,u)/C_P(q^2)=-\frac{q}{2\sqrt{3}M}\left\{\sqrt{\frac{\bar{l}+1}{2\bar{l}+1}}[1\bar{l}+1u+] + \sqrt{\frac{\bar{l}}{2\bar{l}+1}}[1\bar{l}-1u-]\right\}\delta_{\bar{l}u}S'_{0u}(-\kappa). \tag{5}$$

The Gamow-Teller-type term is the first term on the right-hand side of Eq. (4).

In Eqs. (3)–(5), κ labels the quantum numbers of the emitted neutrino ν_λ,

$$\kappa>0: \quad j=l-\frac{1}{2}, \quad l=\kappa, \tag{6}$$

$$\kappa<0: \quad j=l+\frac{1}{2}, \quad l=-\kappa-1, \tag{7}$$

where l and j are the orbital and total angular momentum quantum numbers of ν_λ. The quantity $\bar{l}$ is given by $l-\mathrm{sgn}(\kappa)$, W are the usual Racah coefficients, and

$$S_{ku}(\kappa)=\sqrt{2(2j+1)}\,W(1/2\,1\,j\,l,1/2\,u) \quad (k=1) = \sqrt{\frac{2j+1}{2l+1}} \quad (k=0),$$

$$S'_{ku}(-\kappa)=\mathrm{sgn}(\kappa)S_{ku}(-\kappa). \tag{8}$$

The most important ingredients, the transition operators, are embedded in the reduced matrix elements $[kwu]$, $[kwu\pm]$, and $[kwup]$. The quantum numbers labeling the matrix elements are $\mathbf{k}=\mathbf{s}_\lambda+\mathbf{s}_\nu$, so that $k\equiv|\mathbf{k}|=0$ or 1, and $u\equiv|\mathbf{u}|=|\mathbf{J}_f+\mathbf{J}_i|$ is the tensorial rank of the transition operator. The symbol w is the rank of the spherical harmonics and is therefore related to the parity change. It is given by $w=l$ for $[kwu]$- and $[kwu\pm]$-type matrix elements, and $w=l+1$ or $w=l-1$ for $[kwup]$-type matrix element (k and w must be able to couple to u). The symbol p labels the momentum-dependent operators. The matrix elements with the corresponding single-particle operators are listed in Table I. These operators are further multiplied by the radial wave function of the initial-state lepton [16]. We have taken into account the large component

TABLE I. Reduced nuclear matrix elements and the corresponding single-particle operators [without the lepton radial wave function $G_\mu(r)$]. The $j_w(qr)$ are the spherical Bessel functions and Y^M_{kwu} are the vector spherical harmonics [16]. The momentum operator for nucleons is $\mathbf{p}$, and p_ν is the momentum of the neutrino.

Matrix element	O_{kwu}
$[0wu]$	$j_w(qr)Y^M_{0wu}(\hat{\mathbf{r}})\delta_{wu}$
$[1wu]$	$j_w(qr)Y^M_{1wu}(\hat{\mathbf{r}},\sigma)$
	$O_{kwu\pm}$
$[0wu\pm]$	$[j_w(qr)\pm\alpha Z(m'_\mu/p_\nu)j_{w\mp1}(qr)]Y^M_{0wu}(\hat{\mathbf{r}})\delta_{wu}$
$[1wu\pm]$	$[j_w(qr)\pm\alpha Z(m'_\mu/p_\nu)j_{w\mp1}(qr)]Y^M_{1wu}(\hat{\mathbf{r}},\sigma)$
	O_{kwup}
$[0wup]$	$ij_w(qr)Y^M_{0wu}(\hat{\mathbf{r}})\sigma\cdot\mathbf{p}\delta_{wu}$
$[1wup]$	$ij_w(qr)Y^M_{1wu}(\hat{\mathbf{r}},\mathbf{p})$

$$G_\mu(r)=2(\alpha Z m'_\mu)^{3/2}e^{-\alpha Z m'_\mu r}, \tag{9}$$

where $\alpha\approx1/137$ is the fine structure constant and m'_μ is the reduced muon mass.

The amplitude (2) can be used for the calculations of muon (or electron) capture rates [14,16]. As mentioned in the previous section, our aim is to calculate the effective charges (effective form factors) for the vector, axial vector, and pseudoscalar parts of the amplitude, so as to help to understand the differences between calculated and experimental rates and other observables.

For the actual calculations, we divide the reduced nuclear matrix elements into single-particle and many-body parts,

$$M_\alpha(\kappa,u)=\sum_{pn}[n||m_\alpha(\kappa,u)||p]\frac{(J_f||[a^\dagger_n\tilde{a}_p]^J||J_i)}{\sqrt{2J+1}}, \tag{10}$$

where $n\equiv(n_n,l_n,j_n)$ and $p\equiv(n_p,l_p,j_p)$ label the single-particle states. The doubly barred matrix elements are reduced in the angular momentum space. These reduced single-particle matrix elements, which we calculate in the harmonic oscillator basis with the single-particle operators $m_\alpha(\kappa,u)$, are constructed as described in the following section. Further, we have defined

$$\tilde{a}_{jm}=(-1)^{j+m}a_{j,-m}. \tag{11}$$

As an example, from Eq. (4), the single-particle matrix element for the axial vector part is

$$(n||m_A(\kappa,u)||p) = -C_A(q^2)[n||O_{1lu}G_\mu(r)||p]S_{1u}(\kappa) + \frac{C_A(q^2)}{M}[n||O_{0\bar{l}up}G_\mu(r)||p]\delta_{\bar{l}u}S'_{0u}(-\kappa)$$
$$+ C_A(q^2)\frac{q}{2\sqrt{3}M}\left\{\sqrt{\frac{\bar{l}+1}{2\bar{l}+1}}[n||O_{1\bar{l}+1u+}G_\mu(r)||p] + \sqrt{\frac{\bar{l}}{2\bar{l}+1}}[n||O_{1\bar{l}-1u-}G_\mu(r)||p]\right\}\delta_{\bar{l}u}S'_{0u}(-\kappa). \tag{12}$$

A closer look into the Gamow-Teller-type matrix element gives

$$-C_A(q^2)[n||O_{1lu}G_\mu(r)||p]S_{1u}(\kappa) = -C_A(q^2)i^{l_p-l_n}[l_nj_n||Y_{1lu}(\hat{\mathbf{r}},\sigma)||l_pj_p]$$
$$\times\int_0^\infty r^2R_{n_nl_n}(r)j_l(qr)R_{n_pl_p}G_\mu(r)dr\sqrt{2(2j+1)}\,W(1/2\,1\,j\,l,1/2\,u). \tag{13}$$

Here $R_{nl}(r)$ are the radial single-particle wave functions. The reduced matrix element of the vector spherical harmonics is given by

$$(l_nj_n||Y_{1lu}(\hat{\mathbf{r}},\sigma)||l_pj_p) = \sqrt{\frac{3}{16\pi^2}}(-1)^{l_p+j_p+j_n+l+1}\hat{l}\hat{u}\hat{j}_p\hat{j}_n\begin{pmatrix} j_p & j_n & u \\ 1/2 & -1/2 & 0\end{pmatrix}$$
$$\times\left[\frac{\hat{j}_n^2+(-1)^{j_n+j_p+u}\hat{j}_p^2}{\sqrt{2u(u+1)}}\begin{pmatrix} u & 1 & l \\ 1 & -1 & 0\end{pmatrix} + (-1)^{l_n+1/2+j_n}\begin{pmatrix} u & 1 & l \\ 0 & 0 & 0\end{pmatrix}\right], \tag{14}$$

where $\hat{x}=\sqrt{2x+1}$. The expressions for the vector and pseudoscalar parts are obtained in a similar way using Eqs. (3) and (5) and Table I, where the operators O of Eq. (12) are given. For more details, see [16].

The many-body part, the one-body transition density (OBTD), is given by the adopted nuclear model. The effective operators introduced in Sec. III do not affect the OBTD, which are taken to be given numbers. We do not calculate them here (see, e.g., [14] for examples). In what follows we shall consider only the single-particle part of Eq. (10). This is analogous to, e.g., $M1$ transitions, where the effective charges are calculated without referring to the many-body part.

III. PERTURBATIVE METHODS AND EFFECTIVE OPERATORS TO SECOND ORDER

In order to derive a microscopic approach to the effective operator within the framework of perturbation theory, we need to introduce various notations and definitions pertinent to the methods exposed. In this section we briefly review how to calculate an effective one-body operator within the framework of degenerate Rayleigh-Schrödinger (RS) perturbation theory [17,18]; see also Refs. [6,9] for a detailed discussion on various effective operator diagrams.

It is common practice in perturbation theory to reduce the infinitely many degrees of freedom of the Hilbert space to those represented by a physically motivated subspace, the model space. In such truncations of the Hilbert space, the notions of a projection operator P onto the model space and its complement Q are introduced. The projection operators defining the model and excluded spaces are defined by

$$P=\sum_{i=1}^{D}|\Phi_i\rangle\langle\Phi_i| \tag{15}$$

and

$$Q=\sum_{i=D+1}^{\infty}|\Phi_i\rangle\langle\Phi_i|, \tag{16}$$

with D being the dimension of the model space, and $PQ=0$, $P^2=P$, $Q^2=Q$, and $P+Q=I$. The wave functions $|\Phi_i\rangle$ are eigenfunctions of the unperturbed Hamiltonian $H_0=T+U$, where T is the kinetic energy and U an appropriately chosen one-body potential, that of the harmonic oscillator (HO) in this calculation. The full Hamiltonian is then rewritten as $H=H_0+H_1$ with $H_1=V-U$, V being, e.g., the nucleon-nucleon (NN) interaction or the G matrix to be discussed below. The eigenvalues and eigenfunctions of the full Hamiltonian are denoted by $|\Psi_\alpha\rangle$ and E_α, i.e.,

$$H|\Psi_\alpha\rangle=E_\alpha|\Psi_\alpha\rangle. \tag{17}$$

Rather than solving the full Schrödinger equation above, one defines an effective Hamiltonian acting within the model space such that

$$PH_{\rm eff}P|\Psi_\alpha\rangle=E_\alpha P|\Psi_\alpha\rangle=E_\alpha|\Phi_\alpha\rangle, \tag{18}$$

where $|\Phi_\alpha\rangle=P|\Psi_\alpha\rangle$ is the projection of the full wave function onto the model space, the model space wave function. In RS perturbation theory, the effective interaction $H_{\rm eff}$ can be written out order by order in the interaction H_1 as

$$PH_{\rm eff}P = PH_1P + PH_1\frac{Q}{e}H_1P + PH_1\frac{Q}{e}H_1\frac{Q}{e}H_1P + \cdots . \tag{19}$$

Here we have defined $e=\omega - H_0$, where ω is the so-called starting energy, defined as the unperturbed energy of the interacting particles. Similarly, the exact wave function $|\Psi_\alpha\rangle$ can now be written in terms of the model space wave function as

$$|\Psi_\alpha\rangle = |\Phi_\alpha\rangle + \frac{Q}{e}H_1|\Phi_\alpha\rangle + \frac{Q}{e}H_1\frac{Q}{e}H_1|\Phi_\alpha\rangle + \cdots . \tag{20}$$

In studies of nuclear transitions such as beta decay, the quantity of interest is the transition matrix element between an initial state $|\Psi_i\rangle$ and a final state $|\Psi_f\rangle$ of an operator $\mathcal{O}$ defined as

$$\mathcal{O}_{fi} = \frac{\langle\Psi_f|\mathcal{O}|\Psi_i\rangle}{\sqrt{\langle\Psi_f|\Psi_f\rangle\langle\Psi_i|\Psi_i\rangle}}. \tag{21}$$

Since we perform our calculation in a reduced space, the exact wave functions $|\Psi_{f,i}\rangle$ are not known, only their projections onto the model space. We are then confronted with the problem of how to evaluate $\mathcal{O}_{fi}$ when only the model space wave functions are known. In treating this problem, it is usual to introduce an effective operator $\mathcal{O}_{fi}^{\rm eff}$, defined by requiring

$$\mathcal{O}_{fi} = \langle\Phi_f|\mathcal{O}_{\rm eff}|\Phi_i\rangle. \tag{22}$$

Observe that $\mathcal{O}_{\rm eff}$ is different from the original operator $\mathcal{O}_{fi}$. The standard empirical procedure is then to introduce some adjustable parameters in $\mathcal{O}_{fi}^{\rm eff}$.

The perturbative expansion for the effective operator can then be written in a way similar to Eqs. (19) and (20), i.e.,

$$\begin{aligned}\langle\Psi_f|\mathcal{O}|\Psi_i\rangle = \langle\Phi_f|\mathcal{O}|\Phi_i\rangle &+ \left\langle\Phi_f\left|\mathcal{O}\frac{Q}{e}H_1\right|\Phi_i\right\rangle \\ &+ \left\langle\Phi_f\left|\frac{Q}{e}H_1\mathcal{O}\right|\Phi_i\right\rangle + \left\langle\Phi_f\left|\mathcal{O}\frac{Q}{e}H_1\frac{Q}{e}H_1\right|\Phi_i\right\rangle \\ &+ \cdots .\end{aligned} \tag{23}$$

In Fig. 1 we list all diagrams (except folded diagrams) to second order in the interaction evaluated in this work. We do not include Hartree-Fock insertions. For pure Gamow-Teller- or Fermi-like operators (see, e.g., the review article by Towner [6]), such diagrams are exactly zero. Another feature of, e.g., the Gamow-Teller-type operators is that for several diagrams involving particle-hole contributions, these diagrams are exactly zero unless the particle-hole orbits are spin-orbit partners. This means that for LS-closed-shell nuclei like ^{16}O and ^{40}Ca diagrams like (I)–(VIII) or (XIII)–(XX) are all zero. However, this picture changes when we move to closed-shell nuclei like ^{56}Ni and ^{100}Sn. For Ni the last proton and neutron holes are in the $0f_{7/2}$ single-particle orbit. This means that the $0f_{7/2}$ hole and the $0f_{5/2}$ particle states in ^{56}Ni yield nonvanishing contributions to the Gamow-Teller-type operator from the above-mentioned diagrams. Similarly, in Sn these contributions are represented by the spin-orbit partners in the $0g_{9/2}$ hole and the $0g_{7/2}$ particle states. These spin-orbit partners yield then $1\hbar\omega$ intermediates states. Similarly, we have also spin-orbit partners for particles states outside the model space. These are $0g_{9/2}$ and $0g_{7/2}$ for ^{56}Ni and $0h_{11/2}$ and $0h_{9/2}$ for ^{100}Sn. These $1\hbar\omega$ intermediates states are then responsible for the different quenching of the effective operators in the mass regions of ^{16}O-^{40}Ca and ^{56}Ni-^{100}Sn, respectively.

We end this section with a discussion of how to construct a G matrix. The G matrix enters in turn our perturbative expansion for the effective operator. As is well known in nuclear physics, the NN potential exhibits a repulsive core, which renders any perturbative treatment prohibitive. However, one possible way of overcoming this deficiency is to introduce the reaction matrix G, which accounts for short-range correlations. The G matrix is defined through

$$G = V + V\frac{Q}{\omega - QTQ}G. \tag{24}$$

Here, ω is the energy of the interacting nucleons in a medium and V is the free NN potential. We have assumed that the energy of the intermediate states can be replaced by the free kinetic spectrum T, since these states are predominantly of high excitation energy.

In this work we solve Eq. (24) for finite nuclei by employing a formally exact technique for handling Q, originally presented by Tsai and Kuo [19] and discussed in Ref. [20]. Tsai and Kuo employed the matrix identity

$$Q\frac{1}{QAQ}Q = \frac{1}{A} - \frac{1}{A}P\frac{1}{PA^{-1}P}P\frac{1}{A}, \tag{25}$$

with $A=\omega - T - V$, to rewrite Eq. (24) as

$$G = G_F + \Delta G, \tag{26}$$

where G_F is the free G matrix defined as

$$G_F = V + V\frac{1}{\omega - T}G_F. \tag{27}$$

The term ΔG is a correction term defined entirely within the model space P and is given by

$$\Delta G = -V\frac{1}{A}P\frac{1}{PA^{-1}P}P\frac{1}{A}V. \tag{28}$$

Employing the definition for the free G matrix of Eq. (27), one can rewrite the latter equation as

$$\Delta G = -G_F\frac{1}{e}P\frac{1}{P(e^{-1}+e^{-1}G_Fe^{-1})P}P\frac{1}{e}G_F, \tag{29}$$

with $e=\omega - T$.

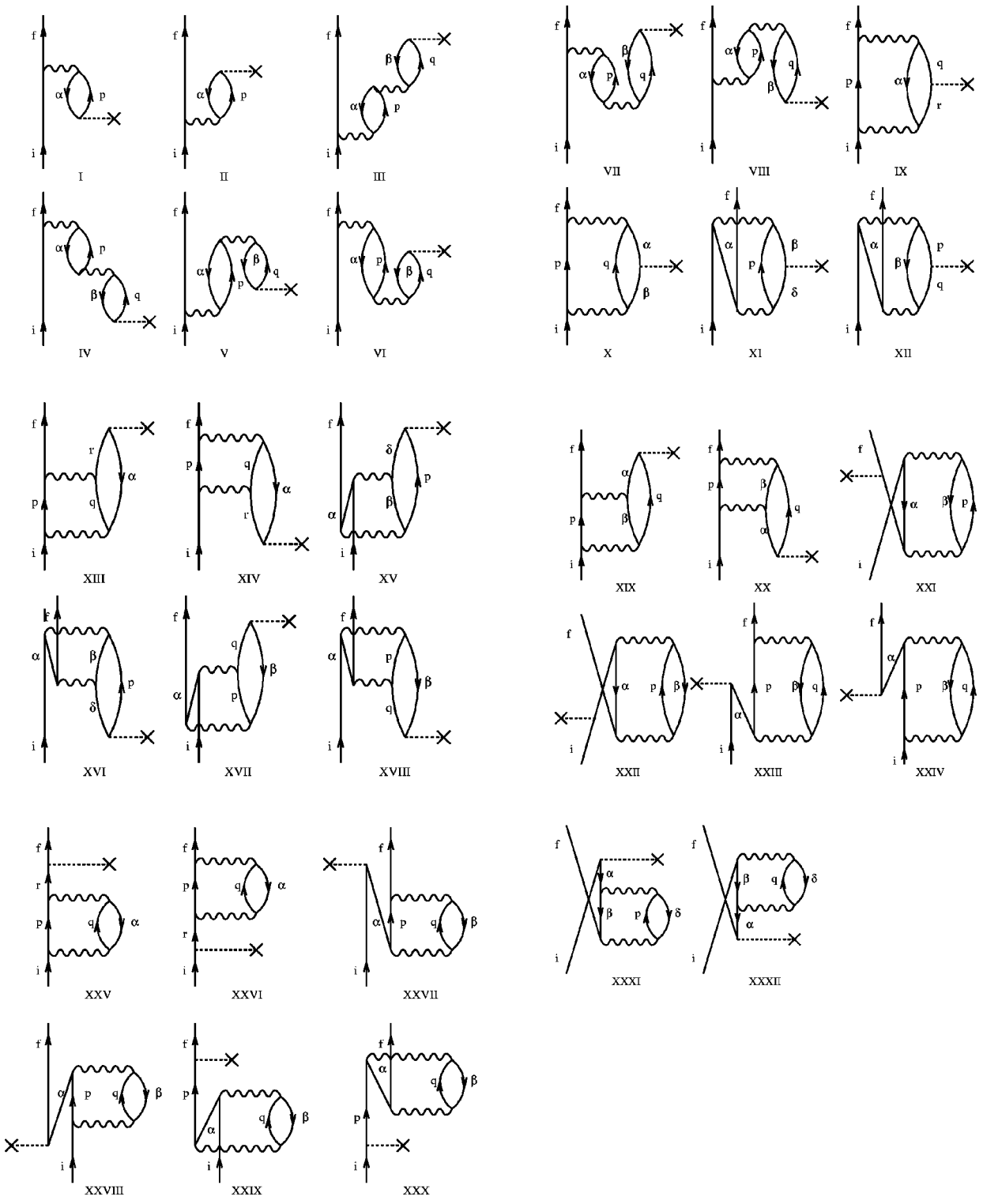

FIG. 1. Nonfolded diagrams to second order in the interaction included in the evaluation of the effective operator. Hole states are represented by greek letters while particle states are given by roman letters. The operator itself is given by $---\times$ in the various diagrams, while the wiggly lines are the nuclear G matrix. Folded diagrams to second order in the interaction are included in the calculation but not shown here.

We see then that the G matrix for finite nuclei is expressed as the sum of two terms; the first term is the free G matrix with no Pauli corrections included, while the second term accounts for medium modifications due to the Pauli principle. The second term can easily be obtained by some simple matrix operations involving the model-space matrix P only.

Finally, in order to calculate the G matrix for the various

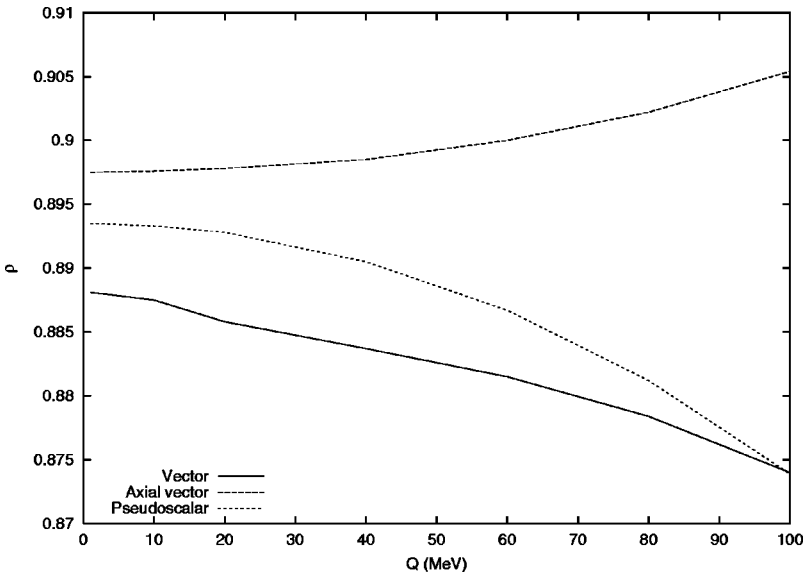

FIG. 2. Renormalization of the vector, axial vector, and pseudoscalar terms with ^{16}O as the closed-shell core, $\kappa=-1$ ($J=0\rightarrow1$ transition, $\Delta\pi=$no).

mass regions, we need to define the relevant model spaces used to define the P and Q operators in the equation for G. The oscillator energies $\hbar\Omega$ will be derived from $\hbar\Omega=45A^{-1/3}-25A^{-2/3}$, A being the mass number. This yields $\hbar\Omega=13.9$, $\hbar\Omega=11.0$, $\hbar\Omega=10.05$, and $\hbar\Omega=8.5$ MeV for $A=16$, $A=40$, $A=56$, and $A=100$, respectively. We choose the model spaces which are believed, from both experiment and theoretical calculations, to be relevant as a first approximation for calculations of effective interactions and operators in the mass areas from $A=16$ to $A=100$. These are the $0d_{5/2}$, $0d_{3/2}$, and $1s_{1/2}$ orbits for $A=16$, the $1p_{3/2}$, $1p_{1/2}$, $0f_{7/2}$, and $0f_{5/2}$ orbits for nuclei in the mass region of $A=40$, the $1p_{3/2}$, $1p_{1/2}$, $0f_{5/2}$, and $0g_{9/2}$ orbits for nuclei in the mass region of $A=56$ and the $0h_{11/2}$, $0g_{7/2}$, $1d_{5/2}$, $1d_{3/2}$, and $2s_{1/2}$ orbits for $A=100$. For these systems, the closed-shell cores (^{16}O, ^{40}Ca, ^{56}Ni, and ^{100}Sn) have equal numbers of protons and neutrons, and the model spaces are the same for both protons and neutrons.

The definition of the Pauli operator for the G matrix can be found in Refs. [20,21], where the so-called double-partitioned scheme has been used. A detailed discussion on the computation of the G matrix can be found in Ref. [21]. This definition means that also the shell above that which defines the model space of the effective interaction is included in the evaluation of the G matrix. For the $1s0d$ shell, this means that we also include the $1p0f$ shell in the definition of the P operator for the G matrix. As a consequence, we have to include in our perturbation expansion ladder type of diagrams where the allowed intermediate states are those of the $1p0f$ shell. With this prescription, we have to evaluate diagrams X, XIII, XIV, and XXIII–XXVIII in Fig. 1.

In our actual calculation of the various effective operators, we truncate the sum over intermediate states at excitations of $(4-8)\hbar\omega$ in oscillator energy. This truncation yields an error of $\sim1\%$ in our evaluation of the effective operator. The nucleon-nucleon interaction employed in this work is the CD-Bonn interaction of Machleidt *et al.* [22].

IV. RESULTS

We consider the transition $0^+\rightarrow1^+$, which is of rank $u=1$. In addition, $\kappa=-1$ or $\kappa=2$, corresponding to $j=\frac{1}{2}$ and $l=0$ or $j=\frac{3}{2}$ and $l=2$, respectively. The nuclear matrix elements, allowed by these quantum numbers together with parity conservation, are $[101]$, $[121]$, $[101-]$, $[121+]$, $[011p]$, and $[111p]$. We remind the reader that the matrix element $[101]$ is closely related to the Gamow-Teller matrix element of the nuclear beta decay, only the radial dependence is more complicated due to the possibility of a larger energy release (see Table I). Our set includes matrix elements which are classified as forbidden in the nuclear beta decay [16].

In order to discuss the average quenching, we define a factor ρ_α:

$$\rho_\alpha(q)\equiv\rho_\alpha=\frac{\sum_{pn}|[n||m_\alpha^{\rm ren}(\kappa,u)||p]|}{\sum_{pn}|[n||m_\alpha^{\rm bare}(\kappa,u)||p]|},\qquad(30)$$

where $\alpha=V$, A, or P, and ''ren'' and ''bare'' refer to renormalized and bare single-particle matrix elements, respectively. The sums run over all the single-particle states included in the model space. We use absolute values in the sums in order to avoid cases where two single-particle matrix elements, with similar magnitudes but opposite signs, cancel each other. This kind of cancellations do not easily happen in nuclear structure calculations, since the involved OBTDs have different magnitudes (and signs).

We start the discussion with $1s0d$-shell nuclei. The effective operators are calculated with $^{16}_{8}$O as a closed-shell core. The model space is the full $1s0d$ shell. From Fig. 2 we see that the quenching for V, A, and P terms remains essentially constant for the whole energy range considered. In particular, at the beta-decay energies (below 20 MeV) all $\kappa=-1$ terms are constant. Moreover, we have $\rho_A^2(0)=0.81$ which is a factor of 2 larger value than the empirical ''universal quenching factor'' of Ref. [11], fitted to a large body of beta-decay data in the $1s0d$ shell (we remind the reader that our effective operators do not include subnucleonic degrees of freedom). We also get a clear renormalization in the vec-

TABLE II. Renormalizations $\rho_A^2(0)$ of selected single-particle transitions. The empirical results from Ref. [10] (^{16}O core) are scaled to $A=17$ [see Eq. (16) in Ref. [10])]. The second line under each entry for the $1s0d$ shell refers, however, to the case where the single-particle orbits are holes with ^{40}Ca as a closed-shell core. The $1p0f$-shell values of this work are for ^{40}Ca as a closed-shell core, except where indicated otherwise. The $g_{9/2}\rightarrow g_{9/2}$ transition is with ^{56}Ni as a closed-shell core. The last four entries are with ^{100}Sn as a closed-shell core.

Transition	This work	Ref. [6]	Ref. [10]	Ref. [24]
$0d_{5/2}\rightarrow 0d_{5/2}$	0.854	0.796 [a]	-	-
	0.823	-	-	-
$0d_{3/2}\rightarrow 0d_{3/2}$	0.832	-	-	-
	0.903	0.681 [a]	-	-
$0d_{5/2}\rightarrow 0d_{3/2}$	0.769	-	-	-
	0.741	-	-	-
$0d\rightarrow 0d$ (average)	0.817	-	0.627	-
	0.821	-	-	-
$1s_{1/2}\rightarrow 1s_{1/2}$	0.778	0.778 [a]	0.656	-
	0.696	0.686 [a]	-	-
$0f_{7/2}\rightarrow 0f_{7/2}$	0.819	0.745 [a]	-	-
$0f_{5/2}\rightarrow 0f_{5/2}$	0.778	-	-	-
$0f_{7/2}\rightarrow 0f_{5/2}$	0.733	-	-	-
$1p_{3/2}\rightarrow 1p_{3/2}$	0.774	0.731 [a]	-	0.593
$1p_{1/2}\rightarrow 1p_{1/2}$	0.869	-	-	-
$1p_{3/2}\rightarrow 1p_{1/2}$	0.745	-	-	-
$0f_{5/2}\rightarrow 0f_{5/2}$	0.210 [b]	-	-	-
$1p_{3/2}\rightarrow 1p_{3/2}$	0.475 [b]	-	-	0.122
$1p_{3/2}\rightarrow 1p_{1/2}$	0.462 [b]	-	-	-
$0g_{9/2}\rightarrow 0g_{9/2}$	0.643	-	-	-
$0g_{7/2}\rightarrow 0g_{7/2}$	0.223	-	-	-
$1d_{5/2}\rightarrow 1d_{5/2}$	0.354	-	-	-
$1d_{3/2}\rightarrow 1d_{3/2}$	0.425	-	-	-
$1d_{5/2}\rightarrow 1d_{3/2}$	0.263	-	-	-

[a]Core-polarization terms only.
[b]With ^{56}Ni as a closed-shell core.

tor and pseudoscalar parts of the current. Note that the CVC hypothesis does not apply here; since we are not looking at Fermi transitions, the vector-type contribution comes from the higher-order terms.

Strictly speaking, our single-particle effective operators are applicable for one-particle systems, e.g., for ^{17}O. In practice, these factors are often used for the whole model space, and the (weak) mass dependence is simply left out. In fact, we find that $\rho_A^2(0)=0.81$ for $^{28}_{14}$Si as well (at the one-particle level). As we average over the single-particle transitions, we believe that the extracted ρ values are representative of the multiparticle configuration mixing calculations. At the end of the model space, effective operators derived for the hole state can also be used. Then, often a larger renormalization compared to the particle operator is seen [6], reflecting the mass dependence. Brown and Wildenthal take this dependence into account by a normalization factor $\propto A^{0.35}$ [10]. In Table II we have added results for the $1s0d$ shell where the single-particle orbits are holes with ^{40}Ca as closed shell core; i.e., our one-particle systems has now $A=39$ rather than $A=17$. One clearly sees a slight enhancement compared to the $A=17$ case, as discussed in Ref. [6] as well. This increase is simply due to the fact that there are more intermediate particle-hole configurations to sum over in the various core-polarization diagrams. Note, however, that relativistic corrections are expected to be larger for hole states than particle states, due to the increased density. Such effects are not accounted for here.

For $^{40}_{20}$Ca as a core, Fig. 3, the overall features are very similar to ^{16}O. We get somewhat more quenching, $\rho_A^2(0)=0.77$. This is in line with earlier studies, where only a slightly larger quenching for the $1p0f$ shell is introduced (see Table II and Ref. [12]). Our model space includes all the single-particle orbits of the $0f1p$ shell. In [12] the authors reach the conclusion that already in the $1p0f$ shell the quenching factor has reached the large-A limit. This is, indeed, confirmed by our results. We also note the good agreement with the results of Ref. [23], Table 1.

As an example, the calculation of Ref. [24] yields $\rho_A^2(0)=0.593$, when two-particle excitations from the $f_{7/2}$ orbit in $0f1p$ space are considered for the $\frac{3}{2}^-\rightarrow\frac{3}{2}^-$ beta decay of ^{57}Cu. Our extracted single-particle quenching $\rho_A^2(0)=0.774$ (with ^{40}Ca as a core; see Table II) is somewhat higher than the quenching stated in Ref. [24]. See, however, below.

Qualitatively, the saturation of the quenching comes from the similar choice of the model space (complete $0\hbar\omega$ space) in ^{16}O and ^{40}Ca. In both cases, the first-order diagrams give zero contribution. Second, particle-hole excitations involving spin-orbit partners are essentially absent. Therefore, typical screening diagram contributions to second-order are negligible (see, e.g., diagrams III–VIII in Fig. 1), and a very similar behavior is expected and, indeed, seen. The differences can be attributed, e.g., to different oscillator parameters and differences in the single-particle orbit structures (in ^{40}Ca more $n\hbar\omega$ excitations are available). Therefore, whenever the model space includes the whole $0\hbar\omega$ oscillator shell, a similar quenching is to be expected. The small variations depend thus on the mass of the closed-shell core.

The model space in which the effective operators are calculated for $^{56}_{28}$Ni does not have a closed LS core. Now, the first-order transitions between $f_{7/2}$, $f_{5/2}$, $g_{9/2}$, and $g_{7/2}$ single-particle orbits become possible (the situation is analogous to the $M1$ operator, which is diagonal in orbital angular momentum and spin). This is clearly reflected in the values shown in Fig. 4. We now have $\rho_A^2(0)=0.56$. We also remind the reader that the Ikeda sum rule for Gamow-Teller (GT) beta decays is not fulfilled in this space. The extreme single-particle model for the beta decay of ^{57}Cu yields a quenching of $\rho_A^2(0)=0.122$ [24]. Our calculation, with ^{56}Ni as a closed-shell core, yields $\rho_A^2(0)=0.475$.

At mass $A=100$ our space includes the single-particle orbits $0g_{7/2}$, $1d_{5/2}$, $1d_{3/2}$, $2s_{1/2}$, and $0h_{11/2}$ above the $N=Z=50$ ($^{100}_{50}$Sn) major shell closure. The spin-orbit partners of $0g_{7/2}$ and $0h_{11/2}$ orbits, $0g_{9/2}$ and $0h_{9/2}$, are missing from our model space. As in ^{56}Ni (see Fig. 5), all terms are

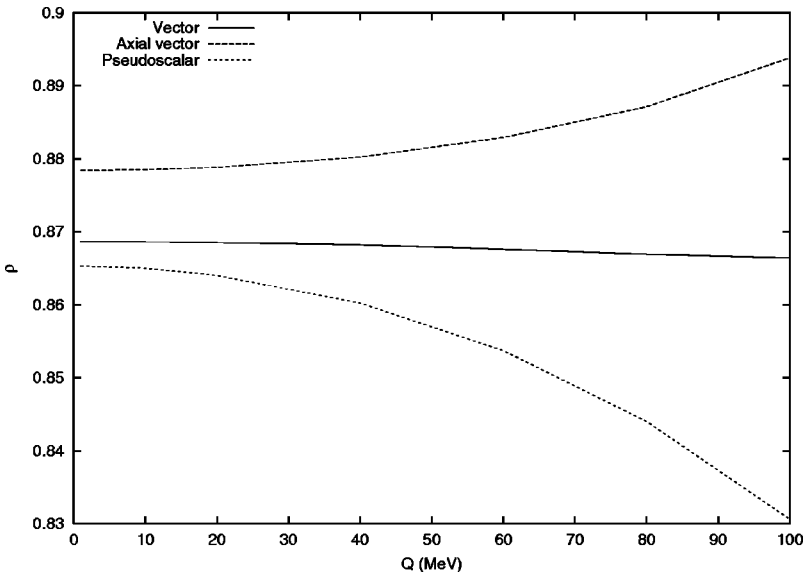

FIG. 3. Renormalization of the vector, axial vector, and pseudoscalar terms with ^{40}Ca as the closed-shell core, $\kappa=-1$ ($J=0\rightarrow1$ transition, $\Delta\pi=$no).

quenched by a factor which is clearly larger than in lighter nuclei with closed LS shells. In the axial vector part we have now $\rho_A^2(0)=0.41$, which again stays nearly constant up to tens of MeVs, well beyond the beta-decay energy range. The kink in the vector curve between $q=80$ and 100 MeV is mainly caused by the increase of the bare $0g_{7/2}\rightarrow0g_{7/2}$ and $0h_{11/2}\rightarrow0h_{11/2}$ transitions.

For nuclei around $A=100$ there is now a wealth of experimental data on β decay; see, e.g., ^{103}In [25] or ^{97}Ag [26]. The β-decay properties are strongly influenced by the transitions between the spin-orbit partners $0g_{9/2}$ and $0g_{7/2}$. Our present model space for ^{100}Sn as a closed-shell core does not include the $0g_{9/2}$ orbit. However, there are also GT transitions which could be described by the present model space. As an example, the Gamow-Teller strength for the reaction ^{127}I$(p,n)^{127}$Xe was recently extracted [27]. The nucleus ^{127}I has been thought of as a candidate for a solar neutrino detector. The theoretical work of Engel *et al.* [28] assumes a quenching factor of 63%–64%, close to ours.

At a single-particle transition level, the spin-flip matrix elements (e.g., $f_{7/2}\rightarrow f_{5/2}$) are more quenched than the diagonal ones. This feature does not depend on the operator or mass. A few examples are shown in Table II, and compared to earlier calculations. We further note that the Gamow-Teller-type matrix element [101], being by far the dominant axial term, follows very closely the trend of the axial vector part through the whole mass range. The l-forbidden single-particle matrix elements ($\Delta l\neq0$) become important in heavier nuclei: The ratio of the reduced axial matrix elements corresponding to transitions $d_{3/2}\rightarrow s_{1/2}$ and $d_{5/2}\rightarrow d_{5/2}$ is 0.0133 with ^{16}O as a closed-shell core. In ^{40}Ca, we have, for the ratio of $f_{5/2}\rightarrow p_{3/2}$ and $f_{7/2}\rightarrow f_{7/2}$ transitions, a value of 0.0145. In ^{100}Sn, we get the ratio of 0.570 for the transitions $g_{7/2}\rightarrow d_{5/2}$ and $g_{7/2}\rightarrow g_{7/2}$. The mass 56 is an intermediate case, since we have the ratio of 0.0827 for the transitions $f_{5/2}\rightarrow p_{3/2}$ and $p_{3/2}\rightarrow p_{3/2}$.

The $\kappa=2$ axial vector terms are shown in Fig. 6. Only the axial vector part is shown, since V and P terms are identical

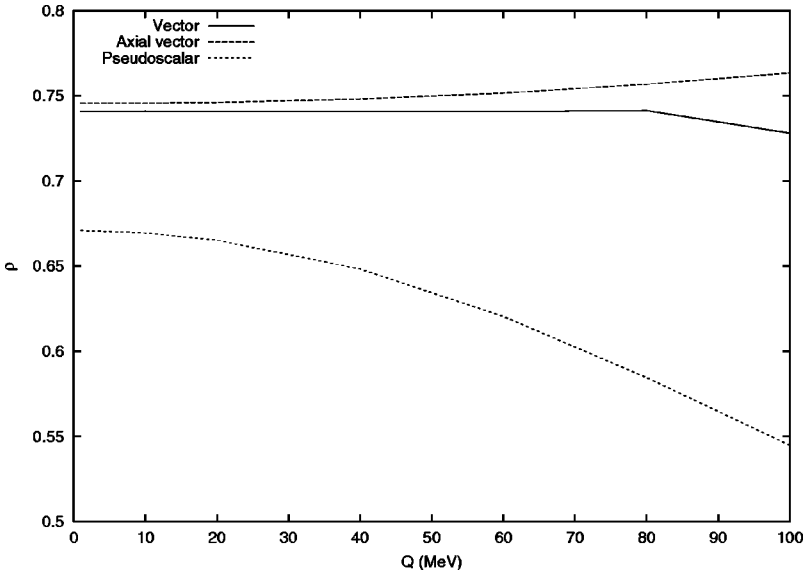

FIG. 4. Renormalization of the vector, axial vector, and pseudoscalar terms with ^{56}Ni as the closed-shell core, $\kappa=-1$ ($J=0\rightarrow1$ transition, $\Delta\pi=$no).

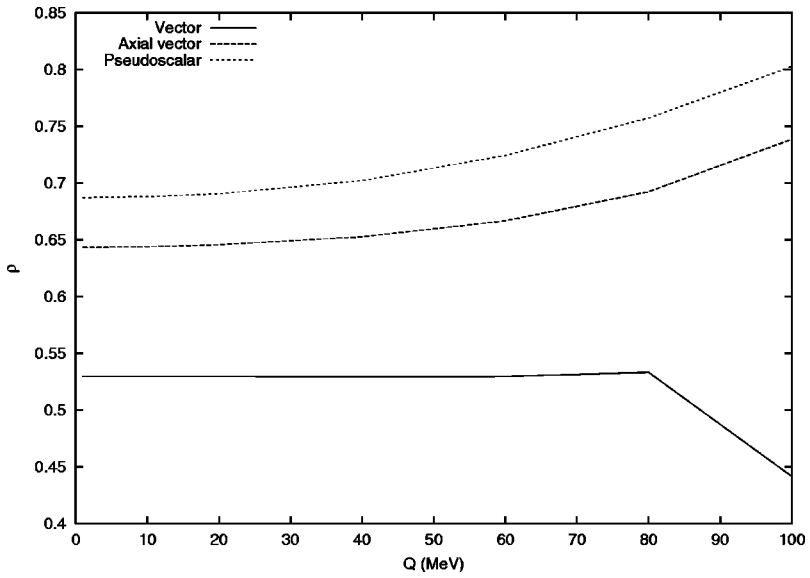

FIG. 5. Renormalization of the vector, axial vector, and pseudoscalar terms with ^{100}Sn as the closed-shell core, $\kappa=-1$ ($J=0\rightarrow1$ transition, $\Delta\pi=$no).

to the case $\kappa=-1$. For $A=16$, 40, and 56 a strong quenching is obtained at high momentum transfers. This is mainly caused by the spherical Bessel function $j_w(qr)$. Oscillations in $\rho_A(q)$ are a sign of the interference between $j_w(qr)$ and the radial single-particle wave function. Clearly, a coherent extraction of the renormalization is not as feasible as in the $\kappa=-1$ case.

In the report by Ciechanowicz *et al.* [29] the meson-exchange contribution to the muon capture matrix elements was found to be very small, at least in capture by ^{28}Si. This is, however, in contrast with the results for $A=12$ nuclei of Ref. [30]. The quenching of the spin matrix element, essentially the Gamow-Teller matrix element, is expected to be dominated by the core polarization correction [6]. However, our results leave some room for subnucleonic corrections. For example, in the $1s0d$ shell, about 50% of the observed quenching [11] comes from Δ isobars, meson-exchange currents, and more complicated many-body terms. The situation is similar also in the beginning of the $1p0f$ shell (^{40}Ca).

Although isobars and meson-exchange currents have been extensively studied in the literature (see, e.g., Ref. [9] for a review), they have been omitted here. The main reason is that we wish to focus on nucleonic contributions only. However, as a result of the way the nucleon-nucleon interaction we employ is parametrized [22], isobars are already included as *implicit* degrees of freedom through intermediate states in, e.g., 2π diagrams. The inclusion of *explicit* isobar degrees of freedom as intermediate states based on a G matrix with one or two isobars as external legs has the potential for double-counting problems. This is the second reason why we have

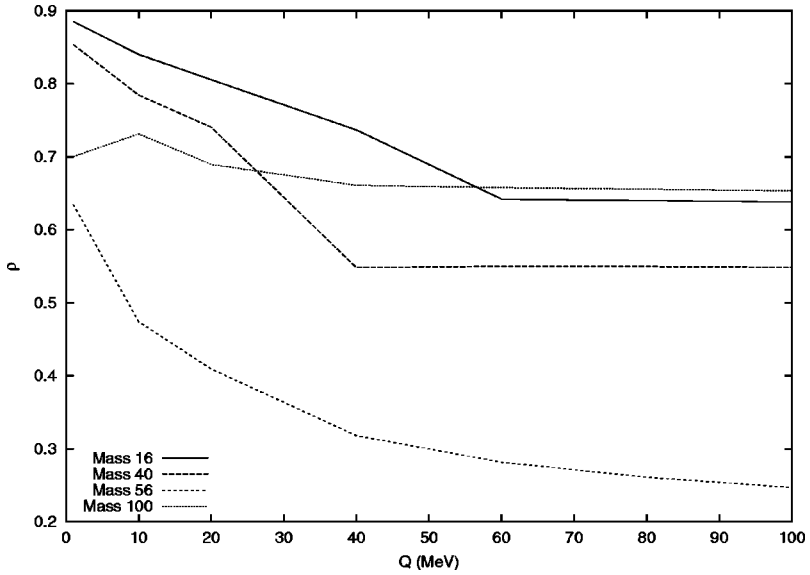

FIG. 6. Renormalization of the axial vector term with $\kappa=2$ for ^{16}O, ^{40}Ca, ^{56}Ni, and ^{100}Sn as closed-shell cores ($J=0\rightarrow1$ transition, $\Delta\pi=$no).

omitted such terms in the present study.[2] However, quite recently, Machleidt has constructed a nucleon-nucleon interaction which includes isobars as explicit degrees of freedom. This interaction [31] accounts for scattering data up to ~ 1 GeV in laboratory energy. We ought, however, to add, that contributions from isobars have essentially been studied through the inclusion of the first-order core-polarization diagram only; see diagrams I and II in Fig. 1 and Ref. [6]. For this diagram the above-mentioned double-counting problems are not important. However, when including isobars as explicit degrees of freedom, it is important that the fitting of the potential include isobars and nucleons on the same footing. That yields an isobar-nucleon interaction which, together with the nucleon-nucleon interaction reproduces, e.g., phase shifts and the binding energy of the deuteron. Finally, we mention that the contribution from second-order diagrams with isobars as intermediate states is an unsettled topic.

The second-order terms in the invariant amplitude describing the process (1) are proportional to M^{-2}. Therefore one would expect their contribution to be at most a few percent of the first order terms [see Eqs. (3)–(5)]. Indeed this is the case. For example, in ^{16}O, the r-dependent single-particle matrix elements, which, according to Barabanov [32], should be the dominating second-order terms, are about an order of magnitude smaller than the first-order terms. Only seldom are the magnitudes roughly equal (one case in ^{16}O). Thus, when the first-order terms are scaled by M^{-1} and second-order terms by M^{-2}, the magnitudes behave roughly as 50:1, respectively. Their contribution is, in this context, neglible. The same conclusion is reached in [32], where detailed expressions for the matrix elements are given.

The quenching factors ρ_A and ρ_P can be used to estimate the ratio C_P/C_A. We take the data from Figs. 2, 3, 4, and 5 at $q=100$ MeV, which corresponds to the muon capture region. Then we have -3.5%, -7.1%, -28.6%, and $+8.7\%$ changes in C_P/C_A for masses 16, 40, 56, and 100, respectively. If the bare value is taken from PCAC, $C_P/C_A \approx 7.0$, we have $C_P/C_A \approx 6.8$, 6.5, 5.0, and 7.6 for masses 16, 40, 56, and 100. This yields an average ~ 6.5. Although not directly comparable to our results, it is interesting to note the results of Kolbe, Langanke, and Vogel [15]. They used the continuum random phase approximation (CRPA) to calculate the part of the capture rate which goes above the particle emission threshold. Their results show a reasonable agreement with data when the bare couplings are used. This nicely demonstrates the fact that if the model space dimension is increased, the couplings should asymptotically reach the bare values. However, the CRPA approach does not include all the higher-order core polarization correlations in the wave functions.

[2]An interesting test case is to calculate the isoscalar part of the $M1$ operator. This term, as demonstrated in Ref. [6], is dominated by core-polarization contributions with nucleonic degrees of freedom only. We have also calculated this operator for single-particle orbits in the $1s0d$ shell with ^{16}O as closed-shell core and find a good agreement (similar to the numbers listed in Table II) with Ref. [6].

V. SUMMARY

We have constructed the effective transition operators corresponding to the general form of the weak hadronic current between the proton and neutron states. The effects of the renormalization are investigated as a function of the transition q value, and an average over the single-particle transitions is taken separately for vector, axial vector and pseudoscalar terms. We have considered only nucleonic degrees of freedom. In addition to the operators present in the allowed beta decay, we have considered the higher-order corrections to the transition amplitudes.

In the $1s0d$ and $1p0f$ shells, we get 19% and 23% quenchings in the axial vector strength, respectively. From these numbers we can conclude that we have reached the large-A limit already in the $1p0f$ shell, supporting the conclusions of [12]. We have also explained this saturation in qualitative terms. In ^{56}Ni and ^{100}Sn, where a major shell closure separates the spin-orbit partners, a larger effect is seen. This is caused by the first-order contributions to the effective operator. The quenching stays nearly constant for energies up to some 60 MeV in all cases. Therefore it is justified to speak about energy-independent quenching factors for beta decays in a given mass region. We also found that the second-order terms (in inverse nucleon mass) are relatively unimportant for most calculations. In particular, the uncertainties in the nuclear model calculations of the one-body transition densities mask these tiny corrections, generally a few percent at maximum.

The quenching factors are used to extract the value of the ratio C_P/C_A at $q=100$ MeV. In light systems such as ^{16}O and ^{40}Ca our results indicate a small (of the order of few percent) quenching. In ^{100}Sn, we obtain an enhancement of the same order of magnitude. In ^{56}Ni a large quenching is seen.

The next step in studies of effective operators is the inclusion of subnucleonic degrees of freedom in the evaluation of the different diagrams entering the definition of the effective operator. Especially we have in mind the Δ isobars as an intermediate state. These states have essentially been neglected due to the lack of a suitable $\Delta\Delta$ interaction. We plan to extend our formalism to include such states through the use of a newly refitted nucleon-nucleon interaction which includes isobars as explicit degrees of freedom. This interaction [31] accounts for scattering data up to ~ 1 GeV in laboratory energy. The inclusion of meson-exchange effects together with the effective transition operators is also a considerable task, not fully attacked yet.

ACKNOWLEDGMENTS

This work has been supported by the Academy of Finland under the Finnish Center of Excellence Programme 2000–2005 (Project No. 44875, Nuclear and Condensed Matter Programme at JYFL).

[1] J. Govaerts, Nucl. Instrum. Methods Phys. Res. A **402**, 303 (1998); Yu. Shitov, Ch. Briancon, V. Brudanin, J. Deutsch, V. Egorov, T. Filipova, J. Govaerts, C. Petitjean, R. Prieels, T. Siiskonen, J. Suhonen, Ts. Vylov, V. Wiaux, I. Yutlandov, and Sh. Zaparov, Nucl. Phys. A (submitted).
[2] R. P. Feynman and M. Gell-Mann, Phys. Rev. **109**, 193 (1958); S. S. Gershtein and Y. B. Zel'dovich, Zh. Éksp. Teor. Fiz. **29**, 576 (1956) [Sov. Phys. JETP **2**, 576 (1956)].
[3] M. L. Goldberger and S. B. Treiman, Phys. Rev. **110**, 1178 (1958).
[4] G. Bardin, J. Duclos, A. Magnon, J. Martino, A. Richter, E. Zavattini, A. Bertin, M. Piccinini, and A. Vitale, Phys. Lett. **104B**, 320 (1981).
[5] D. M. Wright *et al.*, Phys. Rev. C **57**, 373 (1998).
[6] I. S. Towner, Phys. Rep. **155**, 263 (1987).
[7] T. Siiskonen, J. Suhonen, and M. Hjorth-Jensen, Phys. Rev. C **59**, R1839 (1999).
[8] T. Siiskonen, J. Suhonen, and M. Hjorth-Jensen, J. Phys. G **25**, L55 (1999).
[9] B. Castel and I. S. Towner, *Modern Theories of Nuclear Moments* (Clarendon, Oxford, 1990).
[10] B. A. Brown and B. H. Wildenthal, Nucl. Phys. **A474**, 290 (1987).
[11] B. A. Brown and B. H. Wildenthal, Annu. Rev. Nucl. Part. Sci. **38**, 29 (1988).
[12] G. Martinez-Pinedo, A. Poves, E. Caurier, and A. P. Zuker, Phys. Rev. C **53**, R2602 (1996).
[13] M. Karny *et al.*, Nucl. Phys. **A640**, 3 (1998).
[14] T. Siiskonen, J. Suhonen, V. A. Kuz'min, and T. V. Tetereva, Nucl. Phys. **A635**, 446 (1998); **A651**, 437(E) (1999).
[15] E. Kolbe, K. Langanke, and P. Vogel, Phys. Rev. C **50**, 2576 (1994).
[16] M. Morita and A. Fujii, Phys. Rev. **118**, 606 (1960).
[17] T. T. S. Kuo and E. Osnes, *Folded-Diagram Theory of the Effective Interaction in Atomic Nuclei*, Springer Lecture Notes in Physics, Vol 364 (Springer, Berlin, 1990).
[18] I. Lindgren and J. Morrison, *Atomic Many-Body Theory* (Springer, Berlin, 1985).
[19] S. F. Tsai and T. T. S. Kuo, Phys. Lett. **39B**, 427 (1972).
[20] E. M. Krenciglowa, C. L. Kung, T. T. S. Kuo, and E. Osnes, Ann. Phys. (N.Y.) **101**, 154 (1976).
[21] M. Hjorth-Jensen, E. Osnes, and T. T. S. Kuo, Phys. Rep. **261**, 125 (1995).
[22] R. Machleidt, F. Sammarruca, and Y. Song, Phys. Rev. C **53**, R1483 (1996).
[23] I. S. Towner, Phys. Lett. B **333**, 13 (1994).
[24] D. R. Semon *et al.*, Phys. Rev. C **53**, 96 (1996).
[25] J. Szerypo *et al.*, Z. Phys. A **359**, 117 (1997).
[26] Z. Hu *et al.*, Phys. Rev. C **60**, 024315 (1999).
[27] M. Palarczyk *et al.*, Phys. Rev. C **59**, 500 (1999).
[28] J. Engel, S. Pittel, and P. Vogel, Phys. Rev. C **50**, 1702 (1994); Phys. Rev. Lett. **67**, 426 (1991).
[29] S. Ciechanowicz, F. C. Khanna, and E. Truhlik, in *Mesons and Light Nuclei '98*, edited by J. Adam, P. Bydžavský, J. Dobeš, R. Mach, J. Mareš, and M. Sotona (World Scientific, Singapore, 1999), p. 478.
[30] P. A. M. Guichon and C. Samour, Nucl. Phys. **A382**, 461 (1982).
[31] R. Machleidt (private communication).
[32] A. L. Barabanov, Report No. IAE-6119/2, Kurchatov Institute, Moscow, 1999; Yad. Fiz. **63**, 1262 (2000) [Phys. At. Nucl. **63**, 1187 (2000)].